

Rydberg atom reception of a handheld UHF frequency-modulated two-way radio

Noah Schlossberger^{1,*}, Tate McDonald,^{2,1} Nikunj Kumar Prajapati¹, and Christopher L. Holloway¹

¹*National Institute of Standards and Technology, Boulder, Colorado 80305, USA*

²*Department of Physics, University of Colorado, Boulder, Colorado 80309, USA*

 (Received 16 September 2025; revised 18 December 2025; accepted 13 January 2026; published 10 February 2026)

Rydberg atoms, due to their large polarizabilities and strong transition dipole moments, have been utilized as sensitive electric field sensors. While their ability to detect modulated signals has been previously demonstrated, these studies have largely been limited to laboratory-generated signals tailored specifically to atomic detection. Here, we extend the practical applicability of Rydberg sensors by demonstrating the reception of real-world frequency-modulated (FM) audio transmissions using a consumer-grade handheld two-way radio operating in the UHF band. Detection is based on the ac Stark shift induced by the radio signal in a Rydberg atomic vapor, with demodulation performed using an offset local oscillator and lock-in amplification. We successfully demodulate speech signals and evaluate the audio spectral response and reception range. We show that all consumer-accessible radio channels can be simultaneously detected, and demonstrate simultaneous reception of two neighboring channels with at least 53 dB of isolation. This work underscores the potential of Rydberg atom-based receivers for practical, real-world FM signal detection.

DOI: [10.1103/jlrg-6889](https://doi.org/10.1103/jlrg-6889)

I. INTRODUCTION

Alkali atoms in highly excited Rydberg states make sensitive electric field sensors due to their large transition dipole moments and polarizabilities [1]. These quantum field sensors are powerful tools with applications in imaging [2–5] and angle-of-arrival determination [6–13] of rf fields, radar [14,15], and blackbody radiometry [16–18]. One of the largest application spaces for Rydberg sensors is communications. Rydberg atoms are capable of receiving both amplitude- and frequency-modulated signals [19], allowing them to receive signals such as audio [20] and analog video [21]. However, most of these demonstrations have involved detecting a signal that was curated for the Rydberg receiver, with a carrier frequency and modulation scheme chosen to match the capabilities of the sensor. Only a limited body of work [22,23] has examined the use of these atomic sensors to receive real-world signals operating on existing protocols, and these demonstrations have involved collecting the radiation with a classical antenna and focusing it down onto the atomic sensor.

Here we demonstrate that without any focusing or field enhancement, Rydberg atoms can detect the audio signal from a consumer-grade handheld two-way radio or “walkie-talkie.” As these radios transmit in the ultrahigh frequency (UHF) band, we detect their signal by the ac Stark shift they induce on a Rydberg state. This technique is very general as the detection scheme is independent of the carrier frequency. We demonstrate the reception of handheld radio signals with modest postprocessing (only a lock-in amplifier operating at 100 kHz). We also demonstrate that we can simultaneously receive all 22 radio channels, requiring only a separate lock-in filter to decode each channel. We demonstrate this idea by simultaneously and independently detecting two neighboring channels.

II. FRS RADIO

Radio-frequency audio transmission in the UHF band without an operating license in the United States is limited to the Family Radio Service (FRS), which includes the 462.550–462.725-MHz band with an output power limited to 2 W, and the 467.5625–467.7125-MHz band with an output power limited to 0.5 W [24]. These frequency bands are divided into 22 separate channels. The carrier frequencies of each channel are given in Fig. 1(a). The audio is then encoded in a frequency modulation of the carrier. The maximum FM depth, or deviation of the instantaneous frequency from the carrier, is 2.5 kHz, and the maximum FM bandwidth, or encoded audio frequency, is 12.5 kHz.

*Contact author: noah.schlossberger@nist.gov

Published by the American Physical Society under the terms of the [Creative Commons Attribution 4.0 International](https://creativecommons.org/licenses/by/4.0/) license. Further distribution of this work must maintain attribution to the author(s) and the published article’s title, journal citation, and DOI.

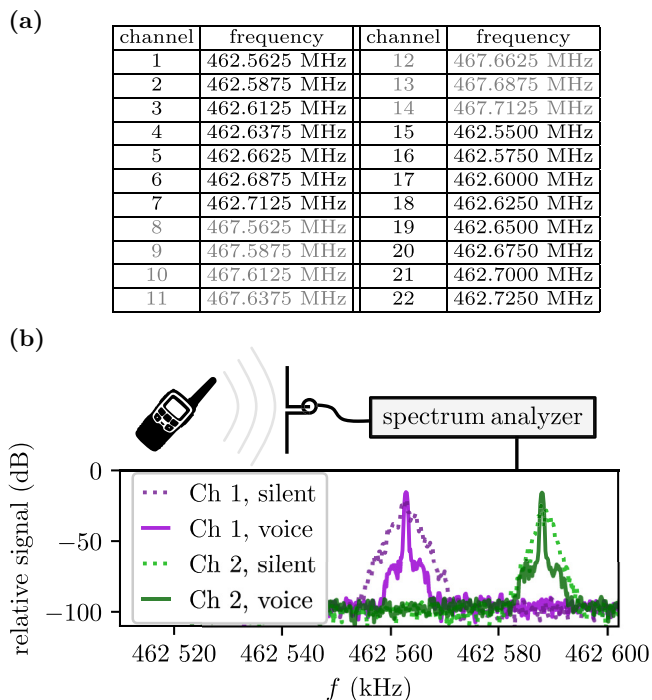


FIG. 1. FRS radio channels. (a) Table of center frequencies of all 22 FRS radio channels. (b) Measured spectrum analyzer traces of the handheld radio transmitting on FRS channels 1 and 2, recorded with a resolution bandwidth of 300 Hz.

In Fig. 1(b) we measure the broadcast of FRS channels 1 and 2 with an unmatched, electrically small dipole antenna feeding into a spectrum analyzer. We transmit using a Midland T51 [25] two-way radio. When the radio operator is silent, no frequency modulation is applied and the signal appears narrowband. When the radio operator speaks, the signal is spread over the bandwidth of the channel. Note that although the signal appears to be many kilohertz wide, the instantaneous frequency is deviating by less than 2.5 kHz (the resolution bandwidth is slow compared with the audio signal).

III. MEASUREMENT SCHEME

To detect FRS radio signals, we use ^{85}Rb atoms as our atomic sensor. We measure the energy of a Rydberg state ($50D_{5/2}$) using a conventional [26,27] two-photon ladder scheme to create an electromagnetically induced transparency (EIT). The energy-level diagram is shown in Fig. 2(a). The two beams are counterpropagating [Fig. 2(b)] in order to partially cancel the Doppler shift due to thermal motion of the atoms, resulting in narrower spectral features.

The 780-nm laser has a beam full width at half maximum (FWHM) of $610\ \mu\text{m}$ and a power of $140\ \mu\text{W}$, while the 480-nm laser has a beam FWHM of $890\ \mu\text{m}$ and a

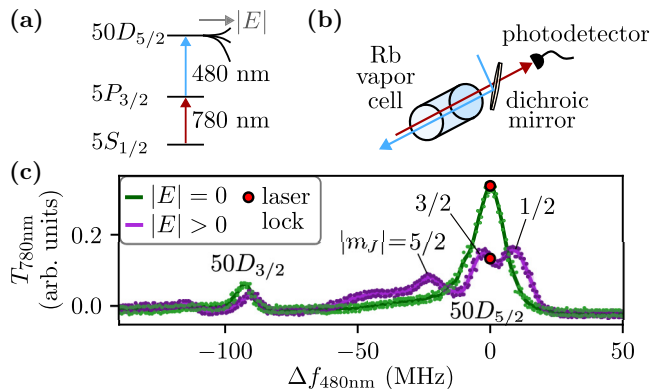


FIG. 2. Measurement of the electric field strength using Rydberg atoms. (a) The energy-level diagram. (b) The physical setup. (c) The measured EIT spectrum, given by the transmission of the 780-nm light ($T_{780\text{nm}}$) as a function of the detuning of the 480-nm light ($\Delta f_{480\text{nm}}$).

power of 490 mW. While beam sizes can affect bandwidth [21], the modulation rates used here (in kilohertz) are much slower than typical atomic response rates (in megahertz), so the beam size requirements are relaxed. The vapor cell is a 25-mm diameter by 72 mm cylinder with 1.5 mm walls. The dimensions of the cell do not matter as they are small compared with the radio signal wavelength (65 cm).

The presence of a UHF band rf field will induce an ac Stark shift on the Rydberg state. To first order, the energy of the Rydberg state is shifted by [28]

$$\Delta U_{\text{Stark}} = \frac{1}{2} \alpha_{|m_J|}(f) E^2, \quad (1)$$

where $\alpha_{|m_J|}(f)$ is the ac polarizability of each fine structure projection m_J state, f is the frequency of the rf field, and E is the root-mean-square (rms) magnitude of the applied electric field. Because each magnitude $|m_J|$ has a different polarizability $\alpha_{|m_J|}$, the rf field will split the spectra into three peaks [Fig. 2(c)]. When we lock the lasers on resonance, a change in the magnitude of the UHF field is mapped into a change in transmission of the 780-nm light [red dots in Fig. 2(c)], and thus a change in the photodetector voltage.

With this scheme, the photodetector voltage tracks the magnitude of the applied field. However, this scheme is insensitive to the frequency of the applied field. The polarizabilities are constant to within a part in 10^8 over the span of one FRS channel [29]. This means that the frequency modulation of the radio signal will not affect the EIT spectrum. In order to detect the FM encoded audio, we apply a local oscillator (LO). The LO interfering with the signal creates a beatnote, acting as a modulation of the rf amplitude, to which the atoms are sensitive. The frequency modulation on the signal is then encoded into frequency

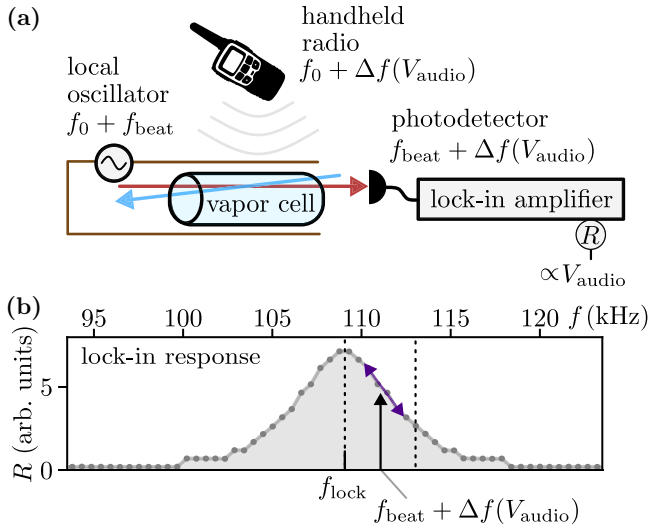


FIG. 3. Demodulation scheme for receiving FM signals via ac Stark shift. (a) The detection scheme. The frequency is denoted at each point along the signal chain to demonstrate the encoding of the audio signal. (b) The lock-in amplifier’s measured amplitude (R) response to various frequencies with the lock-in frequency f_{lock} set to 108.5 kHz. The slope of the response is used to convert the frequency modulation of the beatnote to a voltage.

modulation on the detected beatnote. We apply the LO with an unmatched pair of wires around the vapor cell, creating a localized rf field inside the vapor cell because the electrodes are spaced by much less than a wavelength of the UHF radiation.

The audio detection scheme is shown in Fig. 3. The handheld radio transmits at a center frequency f_0 [as in Fig. 1(a)], with a frequency modulation proportional the audio signal $\Delta f(V_{\text{audio}})$. We then apply a constant tone with an LO a frequency f_{beat} away from the carrier frequency. The two fields interfere inside the vapor cell, resulting in a beatnote between the two fields. This causes the amplitude of the UHF field inside the cell to vary at a beat frequency of

$$|(f_0 + f_{\text{beat}}) - (f_0 + \Delta f(V_{\text{audio}}))| = f_{\text{beat}} + \Delta f(V_{\text{audio}}). \quad (2)$$

This amplitude variation is then mapped to the transmission of the laser light, meaning the photodetector voltage will oscillate at this frequency. With this, we have mapped the frequency modulation of the radio at a carrier f_0 to frequency modulation on the voltage of a photodetector at a carrier f_{beat} .

Finally, to convert the frequency modulation of the beatnote into an audio signal, we use a lock-in amplifier. We select a lock-in frequency f_{lock} slightly different from the beat frequency f_{beat} , so that the signal is sitting on the side of the lock-in amplifier’s response. The response of the lock-in detector then turns the frequency modulation into a modulation on the lock-in amplitude R , which we

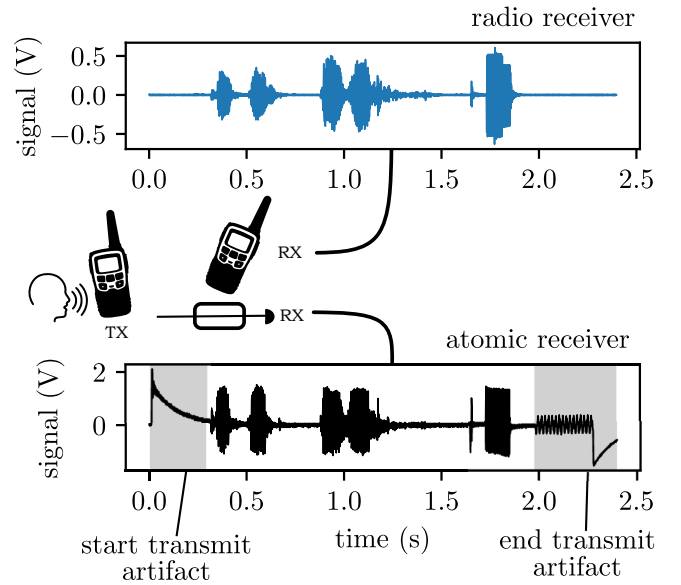


FIG. 4. Simultaneous recordings of a voice speaking into a handheld two-way radio, recorded using the line out of another handheld two-way radio (top) and the atomic receiver (bottom). A recording of the Rydberg-received signal is available [34].

can detect as a voltage from the lock-in amplifier’s R port. This can then be directly connected to speakers or an audio interface.

IV. SINGLE-CHANNEL DETECTION

We demonstrate this scheme by detecting FRS channel 1, with an f_0 of 462.5625 MHz. We choose a beatnote that is fast compared with the audio signal (in kilohertz) such that it can be demodulated, but slow compared with the atomic bandwidth (around 10 MHz [30–33]). We therefore choose a beatnote frequency $f_{\text{beat}} = 111$ kHz, corresponding to an LO frequency of 462.4515 MHz. We then set the data transfer rate of the lock-in amplifier (related to the width of the amplitude response) to 1 kHz, and set f_{lock} to 108.5 kHz (2.5 kHz below f_{beat}). After connecting the amplitude port of the lock-in amplifier to an audio interface, we can record human speech transmitted over the two-way radio (Fig. 4).

The artifacts that occur at the beginning and end of the transmission are due to the turning on and off of the carrier. With no carrier, the value of R will be zero. When the broadcast begins, the carrier generates a finite R , with the audio-induced frequency modulation changing the response of R . This essentially creates a dc bias to the signal, which is removed via ac coupling to the audio interface. When the broadcast begins and ends, this dc bias is suddenly added or removed, which passes through the ac coupling into the audio interface.

Next, we characterize the audio spectral response of the atomic receiver. We connect a function generator to the

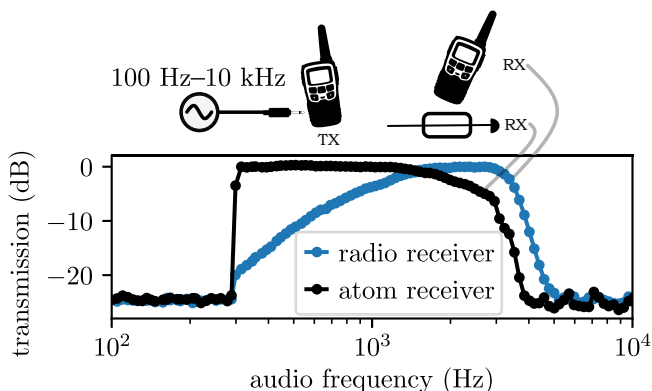


FIG. 5. Spectral response of audio transmitted by a handheld two-way radio and received by either another handheld two-way radio or the atomic receiver. The spectra are normalized to the largest transmitted power to account for different electronic gains of the two receivers.

microphone port of one of the handheld radios to transmit a pure tone, and measure the corresponding transmitted power. The results are shown in Fig. 5.

No transmission occurs below 300 Hz because the two-way radio transmitter does not transmit frequencies below 300 Hz. Over the audio range, the atomic receiver is relatively flat while the radio receiver seems to act as a low-pass filter, most likely due to internal post-demodulation filtering built into the receiver. The radio receiver’s response falls off at around 3 kHz, while the atomic receiver falls off slightly lower at around 2 kHz because the lock-in amplifier’s output has a fourth-order low-pass filter with a 3-dB point at 2 kHz.

Finally, we characterize the range of the atomic radio receiver by measuring the signal-to-noise ratio (SNR) at various ranges (Fig. 6). The SNR is determined by taking the ratio of the rms values of the audio signal during transmission taken during speech versus when not speaking. We then correct for the noise contributing an rms value during speaking by taking

$$\text{SNR}_{\text{corrected}} = \sqrt{\text{SNR}_{\text{uncorrected}}^2 - 1}. \quad (3)$$

Since the audio signal is encoded in the electric field, the strength of the signal will drop off as the strength of the electric field, which goes as $1/r$ where r is the range. Because the detected noise primarily comes from spectroscopic noise which does not scale with range, it is essentially fixed, and so we expect the SNR to fall off as $1/r$. We find in Fig. 6 that the SNR seems to go roughly as $1/r$, but has a large deviation because of reflections in the laboratory as well as variations in the orientation of the handheld radio.

The expected range r to retain an SNR of at least a factor of 2 for a source of directivity \mathcal{D} transmitting a power P from an electrometer of sensitivity \mathcal{S} measuring at a

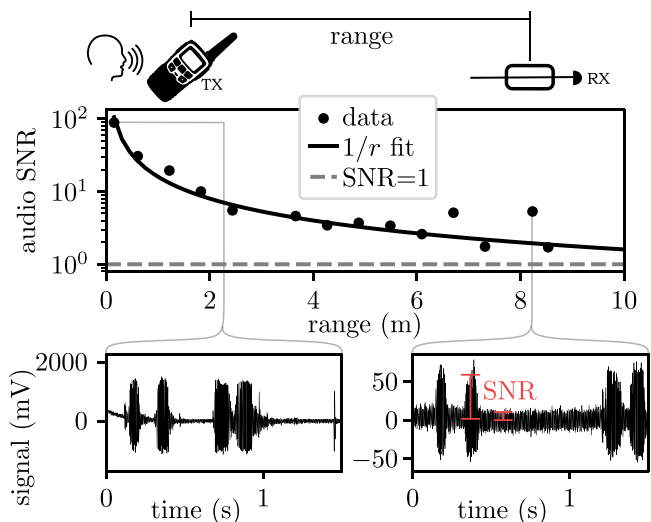


FIG. 6. The signal-to-noise ratio (SNR) of the atomic receiver detecting a two-way radio transmission at varying ranges, corrected as in Eq. (3).

bandwidth of Γ is given by

$$r = \sqrt{\frac{DP}{8\pi c\epsilon_0\Gamma\mathcal{S}^2}}, \quad (4)$$

where c is the speed of light and ϵ_0 is the permittivity of free space. Rydberg electrometers sensing in this regime (frequencies where the ac polarizability approaches the dc polarizability) have been demonstrated with sensitivities as low as $0.1 \text{ mV m}^{-1} \text{ Hz}^{-1/2}$ [35]. Assuming the radio is transmitting at its maximal permitted power ($P = 2 \text{ W}$) and has a Hertzian dipole antenna ($\mathcal{D} = 1.5$), the ideal range we could expect from a Rydberg receiver sampling at $\Gamma = 1 \text{ kHz}$ is 2.1 km. Our Rb state has a lower polarizability than the Cs state used in Ref. [35]; scaling the sensitivity by the polarizabilities of the states, we expect our system to have a maximum ideal range of 40 m, in order-of-magnitude agreement with Fig. 6.

V. MULTICHANNEL DETECTION

Because the 462-MHz portion of the FRS is constrained to a 175-kHz band, which is much less than the instantaneous bandwidth of the Rydberg receiver, every channel in this band will beat against our LO and produce a measurable beatnote on our detector, each at a different frequency. This means that the different channels can be detected simply by changing the frequency f_{lock} of our lock-in detector.

In fact, we can receive multiple channels simultaneously by using multiple lock-in frequencies on our lock-in detector. A scheme of receiving and demodulating multiple FRS channels simultaneously is shown in Fig. 7(a).

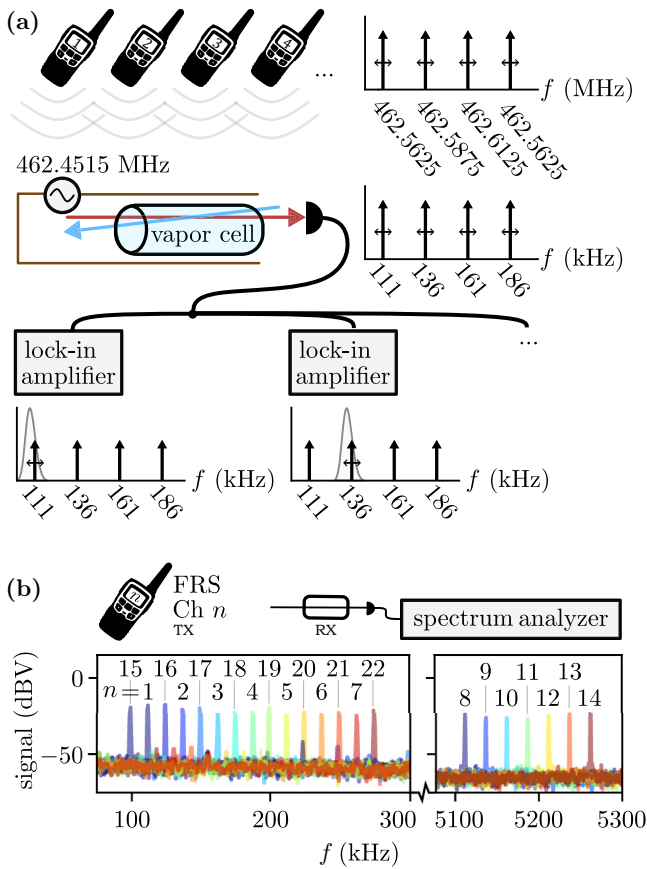


FIG. 7. Measurement scheme for simultaneously receiving all 462-MHz FRS channels. (a) All FRS channels form independent beatnotes with the LO, and each channel is selected and received after the photodiode by different lock-in amplifier channels using different lock-in frequencies. (b) Measured spectrum analyzer traces of the photodetector signal when broadcasting on each FRS channel with the same LO frequency of 462.4515 MHz.

In this scheme, a single LO will automatically generate a separate beatnote for each FRS radio channel, which can be measured by tuning the lock-in amplifier to the channel of interest. Because these beatnotes are independent, multiple channels can be simultaneously received using different channels on the lock-in amplifier. The frequency of the LO relative to the first channel is chosen to be incommensurate with the channel spacing such that harmonics of the beatnotes do not interfere.

To demonstrate the reception of frequency-separated beatnotes for each FRS channel, we measure the photodetector voltage with a spectrum analyzer and record the beatnote signal as we tune the handheld radio to each FRS channel [Fig. 7(b)]. We measure beatnotes in the few-hundred-kilohertz range for FRS channels 1–7 and 15–22, which broadcast at 462 MHz. The other channels still lie within the atomic response bandwidth: we measure beatnotes at 5 MHz for channels 8–14, which broadcast

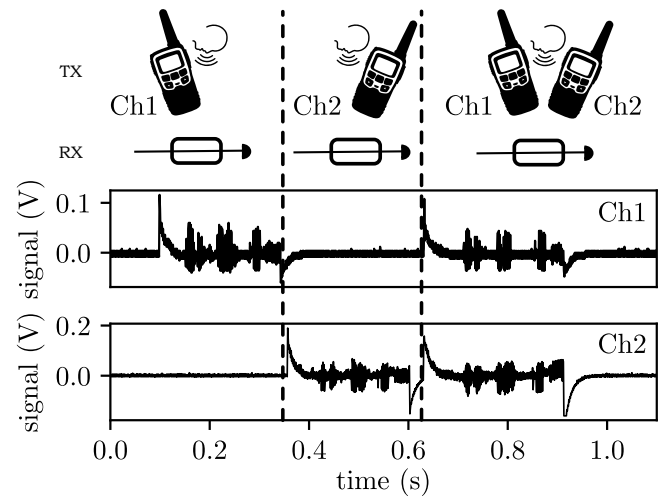


FIG. 8. Simultaneous atomic reception of two FRS channels using two lock-in frequencies on the same photodetector line, with the channel 1 demodulation shown on top and channel 2 on bottom. Three voice transmissions are made, with only channel 1 transmitting (left), only channel 2 transmitting (middle), and both transmitting (right).

at 467 MHz. These could also be demodulated given a high-bandwidth lock-in amplifier.

We demonstrate the simultaneous detection scheme using two handheld radio transmitters and two lock-in amplifier channels. To detect channel 1 ($f_0 = 462.5625$ MHz) and channel 2 ($f_0 = 462.5875$ MHz), we set our LO frequency to 462.4515 MHz and set our lock-in frequencies to 108.5 kHz for FRS channel 1 ($f_{\text{beat}} = 111$ kHz) and 133.5 kHz for FRS channel 2 ($f_{\text{beat}} = 136$ kHz). Both channels use a time constant of 900 samples per second. The recorded audio is shown in Fig. 8.

Here, the two traces represent the two lock-in demodulations. It is qualitatively clear that the two channels are independently received. However, we quantitatively determine the independence of the two channels by broadcasting two separate pure tones (Fig. 9), which we can then separate after reception in Fourier space.

If the channels contained crosstalk, we would detect frequency components of each broadcast in the opposite channel, evident in the power spectral density. We find no crosstalk discernible from the noise floor. As such, the noise floor sets a lower bound on the isolation between channels at 53 dB of isolation from channel 1 into 2 and 40 dB of isolation from channel 2 into channel 1.

VI. CONCLUSION

We have demonstrated reception of FM modulated signals using ac Stark shift in Rydberg states of alkali atoms. We successfully demodulated audio from a handheld consumer two-way radio. We characterized its range and spectral properties. We then demonstrated that we can

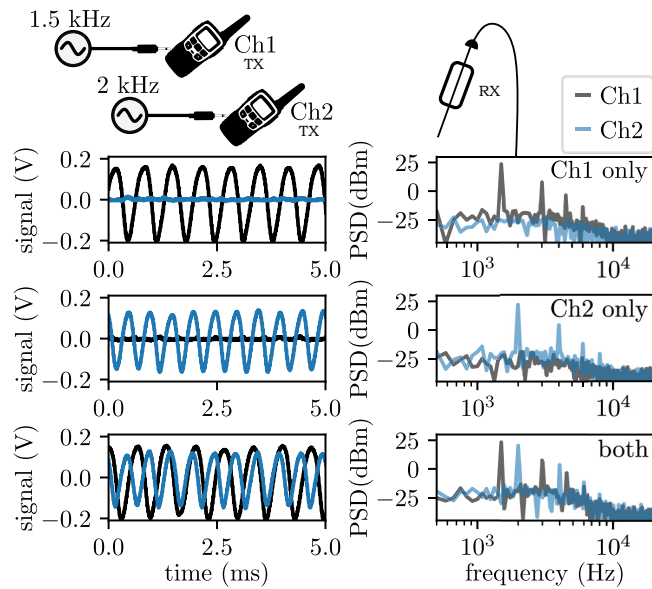


FIG. 9. Measurement of channel isolation during simultaneous detection. The time trace (left) and power spectral density (PSD) (right) are shown when broadcasting a 1.5-kHz pure tone on channel 1 (top), a 2-kHz pure tone on channel 2 (middle), and both simultaneously (bottom).

simultaneously demodulate multiple radio channels, with at least 53 dB of isolation.

While the range we demonstrated was modest, it could be significantly improved with a more sensitive Rydberg state. Cs generally has higher polarizabilities than Rb, increasing further with higher principal quantum numbers. Three-photon systems make Rydberg F -states accessible, which have even higher polarizabilities and resonant transitions in the UHF band [36,37]. In addition, a fiber-coupled probe would allow the vapor cell to be removed from the steel optical table, which attenuates any component of the rf signal whose field is parallel to the surface of the table.

A major drawback of this technique is the requirement of a local oscillator. This could be removed if the Rydberg sensor could be made frequency-dependent. One could imagine placing the vapor cell in a resonant structure such that the amplitude of the field became frequency dependent. However, the width of the resonance would need to be commensurate with the 2.5-kHz frequency modulation depth, requiring a quality factor of the order of 10^4 .

Instead, the practical approach forward would be to choose Rydberg states whose response is frequency dependent in this range. This would eliminate the need for both the LO and the lock-in amplifier, as the frequency-dependent response would map the frequency modulation into a modulation on the strength of the atomic response and the baseband could be directly read out on the photodetector. Three-photon schemes probing F -states can have much lower resonance frequencies than the D -states. For

example, the $56F_{7/2} \leftrightarrow 56G_{9/2}$ transition in ^{85}Rb and the $72F_{7/2} \leftrightarrow 72G_{9/2}$ transition in Cs have resonance frequencies of 469.5 MHz and 464.8 MHz respectively, offering respective polarizability gradients of 0.03% and 0.1% over an FRS channel. However, because the dc polarizabilities of these states are also high, we could introduce a field gradient in the vapor cell by shining visible light to induce the photoelectric effect in alkali atoms adsorbed on the surface [38], which would bring part of the beam into resonance with these transitions. This resonant detection would both be more sensitive and have a much higher frequency dependence, offering a promising path toward FRS radio reception without applying an rf LO.

ACKNOWLEDGMENTS

This research was supported by NIST under the NIST-on-a-Chip program. A contribution of the US government, this work is not subject to copyright in the United States.

The authors declare no conflict of interest.

DATA AVAILABILITY

The data that support the findings of this article are openly available [39].

-
- [1] N. Schlossberger, N. Prajapati, S. Berweger, A. P. Rotunno, A. B. Artusio-Glimpse, M. T. Simons, A. A. Sheikh, E. B. Norrgard, S. P. Eckel, and C. L. Holloway, Rydberg states of alkali atoms in atomic vapour as SI-traceable field probes and communications receivers, *Nat. Rev. Phys.* **6**, 606 (2024).
 - [2] H. Q. Fan, S. Kumar, R. Daschner, H. Kübler, and J. P. Shaffer, Subwavelength microwave electric-field imaging using Rydberg atoms inside atomic vapor cells, *Opt. Lett.* **39**, 3030 (2014).
 - [3] R. Cardman, L. F. Gonçalves, R. E. Sapiro, G. Raithel, and D. A. Anderson, Atomic 2D electric field imaging of a Yagi-Uda antenna near-field using a portable Rydberg-atom probe and measurement instrument, *Adv. Opt. Technol.* **9**, 305 (2020).
 - [4] N. Schlossberger, T. McDonald, K. Su, R. Talashila, R. Behary, C. L. Patrick, D. Hammerland, E. E. Mikhailov, S. Aubin, I. Novikova, C. L. Holloway, and N. Prajapati, Two-dimensional imaging of electromagnetic fields via light sheet fluorescence imaging with Rydberg atoms, *Opt. Lett.* **50**, 7312 (2025).
 - [5] R. Behary, K. Su, N. DeStefano, M. Vorobiov, T. Averett, A. Camsonne, S. Zhang, C. T. Fancher, N. Malvania, E. E. Mikhailov, S. Aubin, and I. Novikova, Electron beam characterization via quantum coherent electric field imaging, *Phys. Rev. Res.* **7**, L042042 (2025).
 - [6] A. K. Robinson, N. Prajapati, D. Senic, M. T. Simons, and C. L. Holloway, Determining the angle-of-arrival of a radio-frequency source with a Rydberg atom-based sensor, *Appl. Phys. Lett.* **118**, 114001 (2021).

- [7] D. Richardson, J. Dee, B. N. Kayim, B. C. Sawyer, R. Wylie, R. T. Lee, and R. S. Westafer, Study of angle of arrival estimation with linear arrays of simulated Rydberg atom receivers, *APL Quantum* **2**, 016123 (2025).
- [8] S. Yan, X. Li, X. Pang, R. Wang, W. Wen, W. Zhai, W. Cui, and Y. Gao, Measurement of Doppler frequency shift and angle of arrival with Rydberg atom-based sensors, *IEEE Trans. Instrum. Meas.* **74**, 1 (2025).
- [9] R. Talashila, W. J. Watterson, B. L. Moser, J. A. Gordon, A. B. Artusio-Glimpse, N. Prajapati, N. Schlossberger, M. T. Simons, and C. L. Holloway, Determining angle of arrival of radio frequency fields using subwavelength, amplitude-only measurements of standing waves in a Rydberg atom sensor, *J. Appl. Phys.* **138**, 114402 (2025).
- [10] R. Mao, Y. Lin, Y. Fu, Y. Ma, and K. Yang, Digital beamforming and receiving array research based on Rydberg field probes, *IEEE. Trans. Antennas Propag.* **72**, 2025 (2024).
- [11] A. Gill, A. Buikema, S. Sirisky, and H. Clevenson, Microwave phase mapping and angle-of-arrival detection using Rydberg atom-based electrometry, [arXiv:2503.22864](https://arxiv.org/abs/2503.22864).
- [12] N. Schlossberger, R. Talashila, N. Prajapati, and C. L. Holloway, Angle-of-arrival detection of radio-frequency waves via Rydberg-atom fluorescence imaging of standing waves in a glass vapor cell, *Phys. Rev. Appl.* **24**, 024056 (2025).
- [13] P. K. Elgee, K. C. Cox, J. C. Hill, P. D. Kunz, and D. H. Meyer, Electrically small Rydberg sensor for three-dimensional determination of radio-frequency k -vectors, *Phys. Rev. Appl.* **23**, 064022 (2025).
- [14] M. Chen, T. Mao, Z. Zhu, H. Feng, G. Gao, Z. Wu, W. Xiao, Z. Li, and D. Zheng, High-resolution quantum sensing with Rydberg atomic receiver: Principles, experiments and future prospects, [arXiv:2506.11833](https://arxiv.org/abs/2506.11833).
- [15] W. J. Watterson, N. Prajapati, R. Castillo-Garza, S. Berweger, N. Schlossberger, A. Artusio-Glimpse, C. L. Holloway, and M. T. Simons, An imaging radar using a Rydberg atom receiver, *Appl. Phys. Lett.* **127**, 161101 (2025).
- [16] D. S. La Mantia, M. Lei, N. Prajapati, N. Schlossberger, M. T. Simons, C. L. Holloway, J. Scherschligt, S. P. Eckel, and E. B. Norrgard, Compact blackbody-radiation atomic sensor: Measuring temperature using optically excited atoms in vapor cells, *Phys. Rev. Appl.* **23**, 044037 (2025).
- [17] N. Schlossberger, A. P. Rotunno, S. P. Eckel, E. B. Norrgard, D. Manchaiah, N. Prajapati, A. B. Artusio-Glimpse, S. Berweger, M. T. Simons, D. Shylla, W. J. Watterson, C. Patrick, A. Meraki, R. Talashila, A. Younes, D. S. La Mantia, and C. L. Holloway, Primary quantum thermometry of mm-wave blackbody radiation via induced state transfer in Rydberg states of cold atoms, *Phys. Rev. Res.* **7**, L012020 (2025).
- [18] S. Borówka, U. Pylypenko, M. Mazelanik, and M. Parniak, Continuous wideband microwave-to-optical converter based on room-temperature Rydberg atoms, *Nat. Photonics* **18**, 32 (2024).
- [19] C. Holloway, M. Simons, A. H. Haddab, J. A. Gordon, D. A. Anderson, G. Raithel, and S. Voran, A multiple-band Rydberg atom-based receiver: AM/FM stereo reception, *IEEE Antennas Propag. Mag.* **63**, 63 (2021).
- [20] C. L. Holloway, M. T. Simons, A. H. Haddab, C. J. Williams, and M. W. Holloway, A “real-time” guitar recording using Rydberg atoms and electromagnetically induced transparency: Quantum physics meets music, *AIP Adv.* **9**, 065110 (2019).
- [21] N. Prajapati, A. P. Rotunno, S. Berweger, M. T. Simons, A. B. Artusio-Glimpse, S. D. Voran, and C. L. Holloway, TV and video game streaming with a quantum receiver: A study on a Rydberg atom-based receiver’s bandwidth and reception clarity, *AVS Quantum Sci.* **4**, 035001 (2022).
- [22] M. Lei, J. Zhang, Q. Luo, Z. Zhang, M. Wang, and M. Shi, Satellite signal detection via Rydberg-atom receiver, [arXiv:2506.15439](https://arxiv.org/abs/2506.15439).
- [23] P. K. Elgee, J. C. Hill, K.-J. E. LeBlanc, G. D. Ko, P. D. Kunz, D. H. Meyer, and K. C. Cox, Satellite radio detection via dual-microwave Rydberg spectroscopy, *Appl. Phys. Lett.* **123**, 084001 (2023).
- [24] Federal Communications Commission (FCC), 47 CFR part 95 subpart B — Family Radio Service (FRS), <https://www.ecfr.gov/current/title-47/chapter-I/subchapter-D/part-95/subpart-B> (2023), accessed: 2025-07-13.
- [25] Certain equipment, instruments, software, or materials are identified in this paper in order to specify the experimental procedure adequately. Such identification is not intended to imply recommendation or endorsement of any product or service by NIST, nor is it intended to imply that the materials or equipment identified are necessarily the best available for the purpose.
- [26] R. Finkelstein, S. Bali, O. Firstenberg, and I. Novikova, A practical guide to electromagnetically induced transparency in atomic vapor, *New J. Phys.* **25**, 035001 (2023).
- [27] A. K. Mohapatra, T. R. Jackson, and C. S. Adams, Coherent optical detection of highly excited Rydberg states using electromagnetically induced transparency, *Phys. Rev. Lett.* **98**, 113003 (2007).
- [28] N. B. Delone and V. P. Krainov, AC stark shift of atomic energy levels, *Phys. Usp.* **42**, 669 (1999).
- [29] E. Robertson, N. Sibalić, R. Potvliege, and M. Jones, Arc 3.0: An expanded Python toolbox for atomic physics calculations, *Comput. Phys. Commun.* **261**, 107814 (2021).
- [30] D. H. Meyer, K. C. Cox, F. K. Fatemi, and P. D. Kunz, Digital communication with Rydberg atoms and amplitude-modulated microwave fields, *Appl. Phys. Lett.* **112**, 211108 (2018).
- [31] J. Hu, Y. Jiao, Y. He, H. Zhang, L. Zhang, J. Zhao, and S. Jia, Improvement of response bandwidth and sensitivity of Rydberg receiver using multi-channel excitations, *EPJ Quantum Technol.* **10**, 51 (2023).
- [32] B. Yang, Y. Yan, X. Li, L. Xiao, X. Li, L. Q. Chen, J. Deng, and H. Cheng, Highly sensitive microwave electrometry with enhanced instantaneous bandwidth, *Phys. Rev. Appl.* **21**, L031003 (2024).
- [33] D. Shylla, N. Prajapati, A. P. Rotunno, N. Schlossberger, D. Manchaiah, W. J. Watterson, A. Artusio-Glimpse, S. Berweger, M. T. Simons, and C. L. Holloway, Observation of asymmetric sideband generation in strongly driven Rydberg atoms, *Phys. Rev. A* **111**, 033115 (2025).
- [34] See Supplemental Material at <http://link.aps.org/supplemental/10.1103/jlrg-6889> for a recording of a human voice

- transmitted by a two-way radio and received using the Rydberg receiver as presented in Fig. 4.
- [35] W. Yang, M. Jing, H. Zhang, L. Zhang, L. Xiao, and S. Jia, Radio frequency electric field-enhanced sensing based on the Rydberg atom-based superheterodyne receiver, *Opt. Lett.* **49**, 2938 (2024).
- [36] R. C. Brown, B. Kayim, M. A. Viray, A. R. Perry, B. C. Sawyer, and R. Wyllie, Very-high- and ultrahigh-frequency electric-field detection using high angular momentum Rydberg states, *Phys. Rev. A* **107**, 052605 (2023).
- [37] N. Prajapati, J. W. Kunzler, A. B. Artusio-Glimpse, A. P. Rotunno, S. Berweger, M. T. Simons, C. L. Holloway, C. M. Gardner, M. S. Mcbeth, and R. A. Younts, High angular momentum coupling for enhanced Rydberg-atom sensing in the very-high frequency band, *J. Appl. Phys.* **135**, 074402 (2024).
- [38] L. Patrick, N. Schlossberger, D. F. Hammerland, N. Prajapati, T. McDonald, S. Berweger, R. Talashila, A. B. Artusio-Glimpse, and C. L. Holloway, Imaging of induced surface charge distribution effects in glass vapor cells used for Rydberg atom-based sensors, *AVS Quantum Sci.* **7**, 024401 (2025).
- [39] N. Schlossberger, Data associated with “Rydberg atom reception of a handheld UHF frequency-modulated two-way radio,” National Institute of Standards and Technology, 2025, <https://doi.org/10.18434/mds2-3947>.